Experimental analysis of the kinetic energy transport and turbulence production in the wake of a model wind turbine

L.E.M. Lignarolo[1], D.Ragni[1], C. Krishnaswami[1], Q.Chen[1,2], C.J. Simao Ferreira[1], G.J.W. van Bussel[1]

[1]Delft University of Technology, Wind Energy, l.e.m.lignarolo@tudelft.nl
[2]Wuhan University, State Key Laboratory of Water Resources and Hydropower Engineering Science

ABSTRACT

The mixing properties of the self-induced flow in a wind turbine wake are studied. The wake of a model horizontal axis wind turbine is analysed with the Particle Image Velocimetry technique and a triple decomposition of the flow. The process of wake re-energising is studied and its dependency on the wake flow structures and stability is shown. The streamwise development of the wake velocity is presented, as well as its clear dependency on the onset of the pairwise instability of the tip-vortices. The mean flow kinetic energy transport and turbulence production is calculated for different regions of the wake. The main conclusion is that the stability of the tip-vortex helix has a strong influence on the mixing of the wake with the outer flow and its re-energising. A thorough estimation of the energy transport at wake scale and the modelling of its dependency on the turbine characteristics would be a first step towards a rotor design process which does not only take into account the aerodynamic and power optimisation of the rotor itself, but also the re-energising properties of the wake, namely the "design of the wake".

Introduction

The wake of a horizontal axis wind turbine (HAWT) is a complex three-dimensional turbulent flow. Its physics has been studied in depth with experiments and field measurements and modelled with numerical analysis. The large inaccuracy in the prediction of loads and energy yields of a wind turbine in a wind farm encountered in the current numerical codes is largely due to the poor modelling of the wake [1], still based on the actuator disc assumption, which does not allow for a correct prediction of the kinetic energy transport and turbulence creation in the flow of a turbine's wake, as shown in [9] . These factors are of paramount importance, because turbulent mixing governs the re-energising process of the wake. In a large wind farm, the energy is provided mainly by the entrainment of high kinetic energy air from the flow above the wind farm itself, apart from the front rows, as demonstrated in previous studies [2]. This phenomenon happens at two different levels: at the atmospheric turbulent flow level and at the wake-induced level. The second one is of particular interest because it concerns the mixing process owing to the presence of the tip vortex helix, its instability and its breakdown, namely parameters which are directly depending on the turbine design and its operation. This becomes even more important for off-shore wind farms, where the role of atmospheric turbulence is much lower than on-shore. However, currently there is no model which allows to quantify the wake induced mixing, nor there is a detailed set of experimental observations in controlled conditions for understanding the physics of this phenomenon and validating a possible model.
Previous studies focussed on the self-induced mixing properties of the wake can be found in [3], [6] and [11], who demonstrate how different turbine parameters affect the wake development in terms of wake stability. [7] makes the hypothesis that the near wake tip vortices prevent the wake to mix with the outer air, but the quantification of the effect of the vortices and their break-down in terms of energy transport is not in his focus; also, this assumption seems to be in contradiction with previous statements of [5], who says that the tip vortices are contributing to the entrainment of air in the wake. [4] demonstrates the importance of vertical transport of kinetic energy to replenish the wakes and to enable the power extraction in the array. This inspiring study is focussed on analysing the mixing

process due to the large scale atmospheric turbulence and its effect on the smaller scale flow structures within a wind farm. In the present project, the environment turbulence is not taken into consideration, in order to study the mixing properties of the wake *per se*, solely caused by the wake induced flow. To the authors knowledge, there is no available study on the effect of the different wake flow structures on the kinetic energy balance of the wake itself and that shows what is their dependency on the turbine characteristics.

The aim of this project is to visualise the dependency of the wake re-energising on the tip vortex helix instability and breakdown. An experimental study is conducted to characterise the evolution of the vortex structures in the wake of a 60 centimetres-diameter two-bladed HAWT model. The measurements are performed in the Open Jet Facility (OJF) wind tunnel of Delft University of Technology and a high-resolution Stereo Particle Image Velocimetry (SPIV) system is used to achieve detailed flow measurements. The wake is measured up to 4 diameters downstream. The zone of interest in the present paper however is up to 2.7 diameters. The wake recovery is estimated in terms of wake velocity and its clear dependency on the onset of wake instability is shown. The wake mixing is determined in terms of mean flow kinetic energy transport. The turbine's wake velocity field u_i is decomposed according to [8] as $u_i = \overline{u_\iota} + \widetilde{u_\iota} + u'_i$ .The terms in the right hand side indicate respectively the mean flow, the periodically fluctuating coherent structures (tip vortices) and a random fluctuating component (turbulence). The phase-locked mean flow kinetic energy transport equation for inviscid flow is:

$$\left(\overline{u_\jmath} + \widetilde{u_\jmath}\right)\frac{\partial \overline{KE}}{\partial x_j} = -\left(\frac{\partial \overline{p u_\iota}}{\partial x_i}\right) - \overline{u_\iota}\frac{\partial \overline{u_\iota}}{\partial t} - \overline{u_\iota}\overline{u_\jmath}\frac{\partial \overline{u_\iota}}{\partial x_j} - \left(-< u_i{}' u'_j > -\widetilde{u_\iota}\widetilde{u_\jmath}\right)\frac{\partial \overline{u_\iota}}{\partial x_j} - \frac{\partial}{\partial x_j}\left[\overline{u_\iota} < u_i{}' u'_j > + \overline{u_\iota}\left(\widetilde{u_\iota}\widetilde{u_\jmath}\right)\right]. \text{ Eq. 1}$$

where <-> indicates the phase-locked average of the quantity, the kinetic energy is $\overline{KE} = \frac{1}{2}\overline{u_\iota}\overline{u_\iota}$, p is the barometric pressure and $\widetilde{u_\iota}\widetilde{u_\jmath}$ and $u_i{}' u_j^{'}$ are respectively the Reynolds stresses due to coherent and incoherent fluctuations. The most important terms to be calculated are the fourth and the fifth term of Eq.1's right-hand side, which represent respectively the mean flow kinetic energy loss into turbulence and vortices and the kinetic energy transport due to the periodic vortices and the turbulence. the latter is represented by a gradient of kinetic energy fluxes. The fourth term can also be written substituting the mean velocity with the phase-locked average velocity and discarding the periodic contribution, obtaining the equation of the turbulence kinetic energy production in one phase. This is shown in Equation 2 in the x-y plane:

$$\langle Pe \rangle = -u'^2\frac{\partial \langle u \rangle}{\partial x} - v'^2\frac{\partial \langle v \rangle}{\partial y} - u'v'\left(\frac{\partial \langle u \rangle}{\partial y} + \frac{\partial \langle v \rangle}{\partial x}\right). \qquad \text{Eq. 2}$$

In this paper it will be shown how the kinetic energy transport is strongly dominated by the disruption of coherence of the vortical structures in the wake. The objective for the near future is to quantify these terms for both a wind turbine rotor's and a porous disc's wake (simulating the actuator disc used in numerical models) and to show the differences in the process of kinetic energy entrainment and destruction (turbulence production) along the two wake's shear layers. This will help understanding the limitations in the current wake models, based on the actuator disc assumption, and will help researchers to understand what level of accuracy (and at what flow scale) the future improved models must have for correctly simulating the wake effect in large wind farms. Ultimately, this will extend the knowledge on the wake re-energising properties for exploiting them in the future wind turbine and wind farm design.

Experimental setup

Wind tunnel and measurement conditions

Experiments have been conducted in the closed-loop open jet wind-tunnel of Delft University of Technology. The wind-tunnel has an octagonal nozzle with an equivalent diameter of 3 m and a contraction ratio of 4:1. Powered by a 500 kW motor, the wind tunnel can achieve a maximum velocity of 34m/s (120kmph). It provides a uniform flow with 0.5% turbulent intensity. The uniform velocity area contracts with a 4.8° semi-angle, due to the shear layer at the boundary of the jet. The flow temperature is kept constant through a heat exchanger which provides up to 350 kW of cooling power. In a previous experimental campaign, aimed analysing the wind tunnel flow oscillations, the stable jet length has been establish as long as 3m from the exit, corresponding to 5 turbine diameters.

Tip Speed Ratio [-]	Frequency of wind turbine [Hz]	Wind speed [m/s]	Thrust coefficient [-]
4.8	9.67	3.8	0.82
6	18.00	5.7	0.89

Table 1: test cases

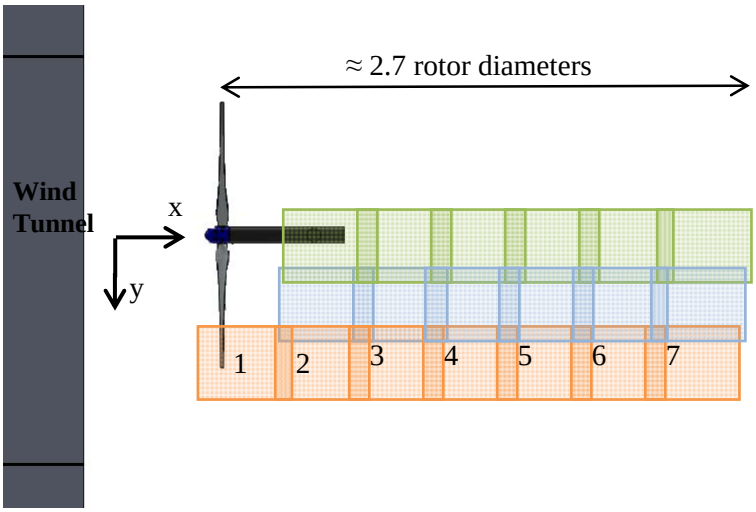

Figure 1: measurement matrix

The measurements were performed on the wake of the wind turbine up to 4 rotor diameters. In this paper the results up to 2.7D are presented as shown in Figure 1. Each window represents a field of view (FOV) in a plane parallel to the ground at the hub height; the darker shade between the windows shows the overlap between two adjacent FOV, which varies from 97 mm to 147 mm in the x direction. The flow was also captured at two inboard positions A and B with an overlap of 102 mm to 98 mm respectively. The measurements were performed in unconditioned sampling and in phase-locked for different azimuthal positions of the blades (-5, 0 and 5 degrees), using an optical trigger positioned inside the nacelle. The device provides one pulse for each rotation and triggers the laser and the cameras. By changing the trigger delay, different phases can be captured. The distance between the turbine and the wind tunnel exit is approximately 0.5 rotor diameters.

Wind turbine model

The wind turbine used in the experiment is a 2-bladed wind turbine with a design tip speed ratio of 6. The rotor radius is 30cm (which provides a low model to tunnel area ratio of 0.04) with a maximum twist of about 18.0 degrees at the root and a minimum twist of 4.4 degrees at the tip. The maximum chord of the blade is 7.4 cm which occurs at a distance of 5.5 cm from the axis. An Eppler E387 [10] airfoil with a thickness to chord ratio of 9.06% is used along the blade span. The Reynolds number at the tip region is about 100,000 at TSR=6. The twist and chord distribution are shown in Figure 2. The nacelle is designed in order to be compact, so that its effect on the flow is minimal. The nacelle which occupies about 6% of the total diameter, houses a DC brushless motor, a gearbox, a hall encoder and the optical trigger. The turbine is mounted on a tower which is 3m tall.

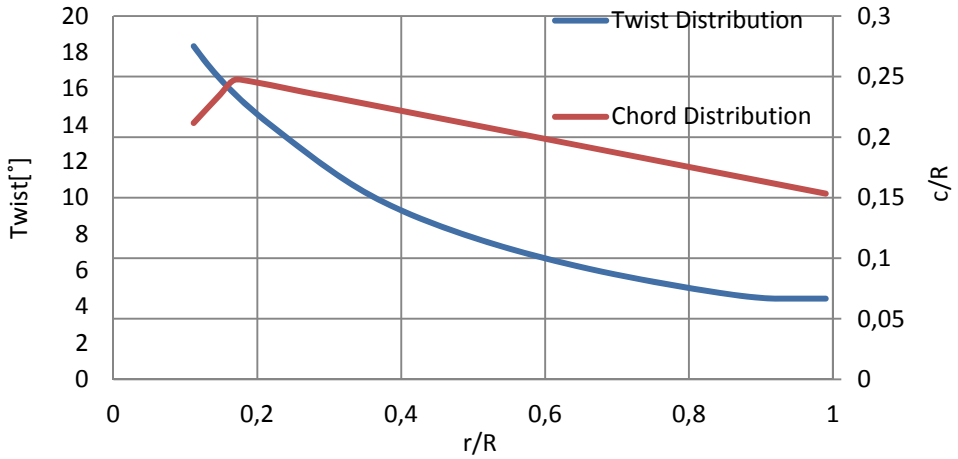

Figure 2: Blade Characteristics

Stereo Particle Image Velocimetry

A stereoscopic PIV setup has been installed in a traversing system able to scan the flow field in the wake of the horizontal-axis wind-turbine wake. The required illumination is provided by a Quantel Evergreen Nd:YAG laser system with 200 mJ/pulse energy at a max frequency of 15 Hz (527 nm wavelength). The laser light is conveyed to form a 2 mm laser sheet of about 35 cm width at the field of view, by combination of a spherical lens of focal f = -50 mm and two cylindrical lenses of f = +80 mm and f = -40 mm. Two LaVision Imager Pro LX 16 Mpix (4870 × 3246 px^2, 12 bits) with pixel pitch of 7.4 μm/px are used to image a field of view of 357 × 253 mm^2, obtained with two Nikon lenses of f = 180 mm and aperture f# = 2.8 - 4, at a magnification M of 0.10 The focusing plane has been slightly offset with respect to the laser plane (defocusing), to obtain an image of the particle of about 2-3 px, to mitigate the bias errors associated with peak locking [13]. Seeding was provided in the test section by a SAFEX smoke generator with SAFEX MIX, able to produce liquid droplets of less than 1 μm. The entire setup was mounted on a traversing system able to translate in two directions. Ensemble of 400 (phase-locked), 720 (unconditioned) double-frame recordings have been acquired and processed by LaVision Davis 8.1.4. Interrogation windows of 24 × 24 px^2 with 50% overlap allows to have a vector resolution of 1.76 mm, and a vector pitch of 0.88 mm.

The laser control, camera synchronization, and image acquisition are triggered by an opto-coupler TCST 2103, together with a disc perforated at a specific azimuthal position and rotating with the

turbine's shaft providing a one-pulse digital signal for each rotation. The cameras and the laser are mounted on the same structure which in turn is mounted on a traversing system, thus guaranteeing the same setup while the traversing systems travels.

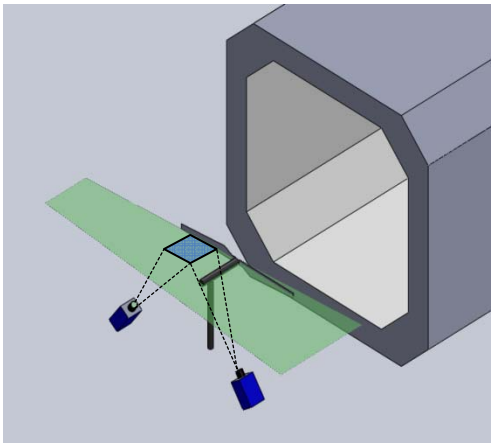

Figure 3: Setup for wake location

Separation Time between the images	200μs
Final interrogation window size	24 x 24
Number of Images	For phase locked sampling: 400 For unconditioned sampling: 720
Pixel size	0.0074 mm/px

Table 2: PIV parameters

Experimental results

In this section, the near- and transition- wake velocity fields till ~2.7 diameters downstream are shown for two different tip-speed ratios. Results are both for phase–locked and unconditioned sampling, namely representing the phase-locked average velocity field and its unconditioned average on all phases. Figure 4 depicts the normalised axial velocity field in the shear layer between the wake and the outer flow till about 1.6 metres (~2.7 diameters) downstream averaged on all phases. The most evident feature in these plots is the location of the wake breakdown, where vortices start a pairwise interaction, the so-called leapfrogging, as shown also in [3,11] and presented later in this paper. In the average field, this appears as a sudden enlargement of the shear layer, starting at ~1 diameter downstream for TSR=6 and ~1.3 diameters downstream for TSR=4 and reaching its maximum at ~1.4 diameters for TSR=6 and at ~1.7 diameters for TSR=4.8. The onset of wake instability is therefore clearly depending on the TSR as shown in [5]. Figure 5 shows the phase-locked velocity field of the shear layer and the inboard region till the hub centreline. The evolution of the tip vortex is shown and the pairwise interaction is now evident. In this picture the nacelle's wake is visible in the inboard region. It is also evident how the tip-vortex has almost completely diffused after the first leapfrogging. This would suggest a strong influence of the large scale wake instability on the tip-vortex diffusion. This hypothesis will be addressed in future studies. Figure 6, depicting the streamwise profiles of axial velocity at different radial locations, shows that the re-energising process starts right after the instability around locations ~1.4 diameters for TSR=6 and at ~1.7 diameters for TSR=4.8. Comparing Figure 6 and Figure 5, it is clear that the onset of the re-energising process coincides with the location of the leapfrogging event. After reaching a minimum at the maximum wake expansion, the axial

velocity intakes a process of re-energising, starting from the outer regions where the turbulent mixing with the external flows happens as evident in Figure 7.

In Figure 8 and 9 the terms $\overline{u_i}\left(\widetilde{u_i}\widetilde{u_j}\right)$ and $\overline{u_i}\langle u_i{}'u_j'\rangle$ of Equation 1 in the x-y plane (namely $\bar{u}(\tilde{u}\tilde{v})$ and $\bar{u}\langle u'u_j'\rangle$) are estimated. These represent the fluxes of mean-flow kinetic energy by means of the periodic vortices and the turbulence respectively. Positive values mean downward fluxes of kinetic energy. Two zones can be identified. The first zone, where the wake expansion occurs, shows the tip-vortices structures to be the only structures determining a mean flow kinetic energy transport across the wake layer, although with a zero net value. The second zone, after the onset of the wake instability, is characterised by a downward net entrainment of kinetic energy, i.e. towards the inner region of the wake., signifying a dominant role of incoherent structures in the mean flow kinetic energy transport and therefore in the re-energising process. The finding is in accordance with the hypothesis of Medici (2005) who stated that the near wake tip-vortices are acting as a shield preventing the wake to mix with the outer flow. Figure 10 shows the production of turbulent kinetic energy, which constitutes a sink of mean flow kinetic energy. Equation 2 describes the process of destruction of the phase averaged flow kinetic energy by mean of the turbulent fluctuations. Again, it is possible to see how the generation of turbulence becomes more violent in the downstream regions after the instability.

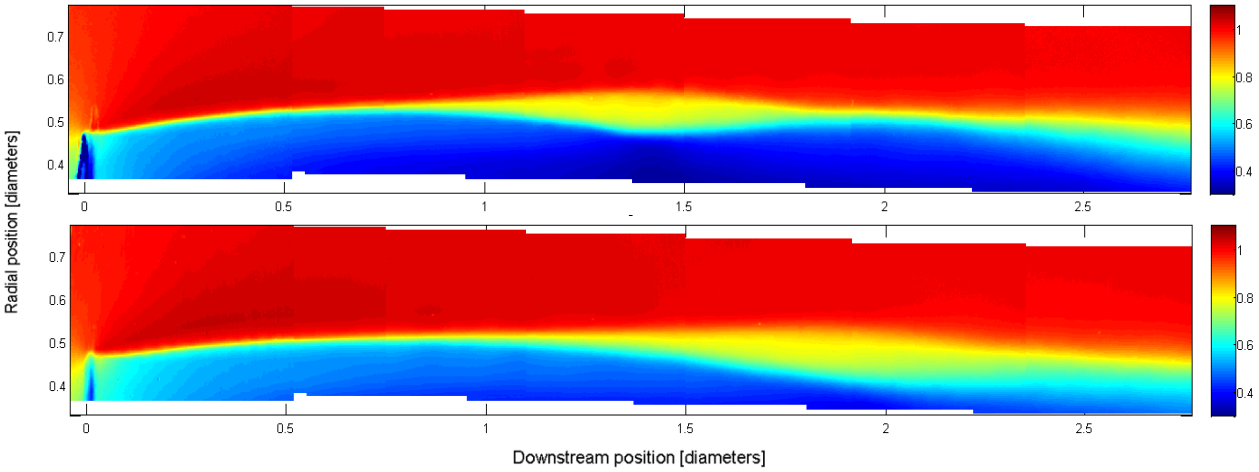

Figure 4: normalised average axial velocity field $\bar{u}/U_{inf}$ in the wake shear layer till 2.7 diameters downstream at two different tip-speed ratios; (up)TSR=6; (down)TSR=4.8

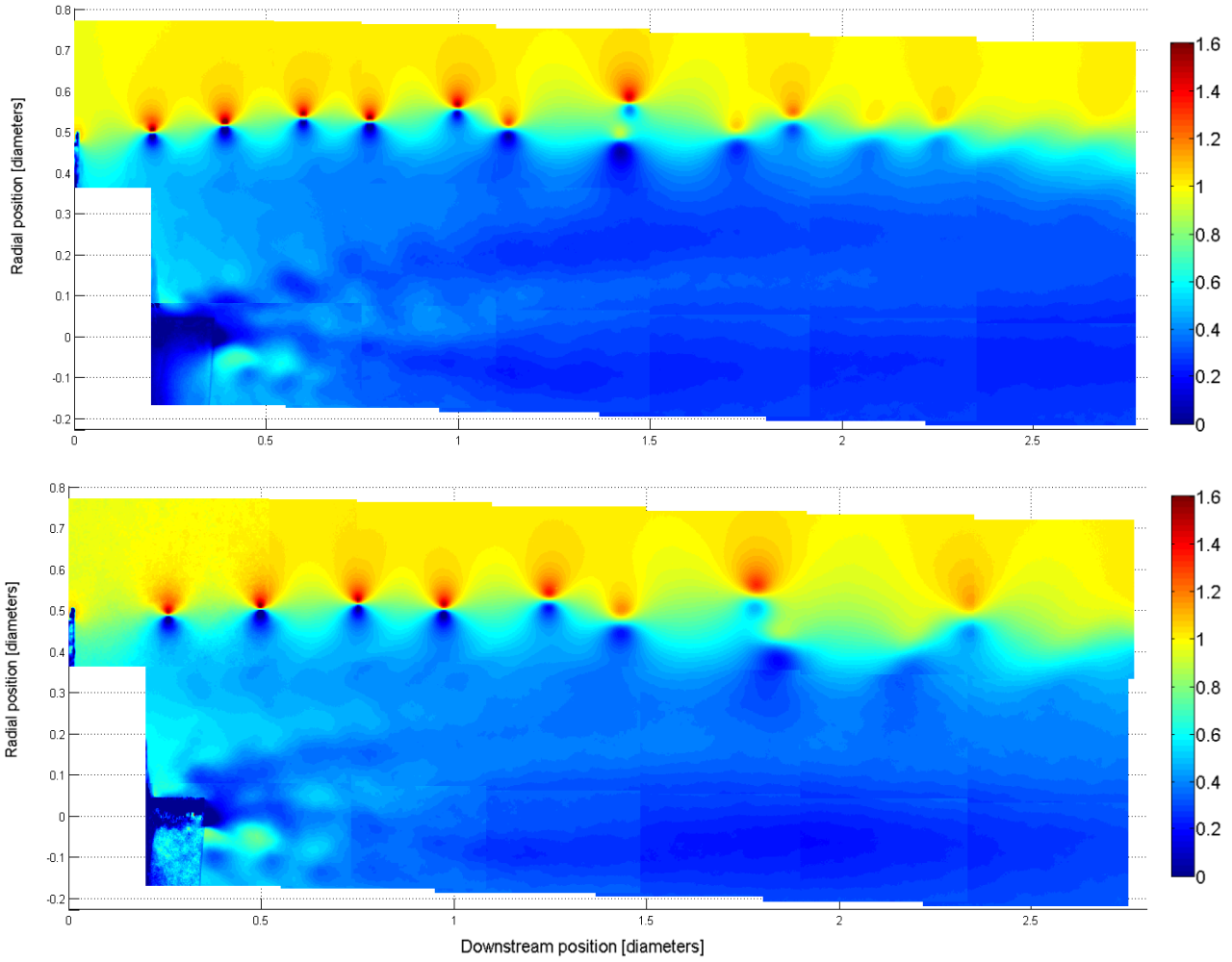

Figure 5: phase-locked averaged normalized axial velocity field $\langle u \rangle / U_{inf}$ for TSR=6 (up) and TSR=4 (down)

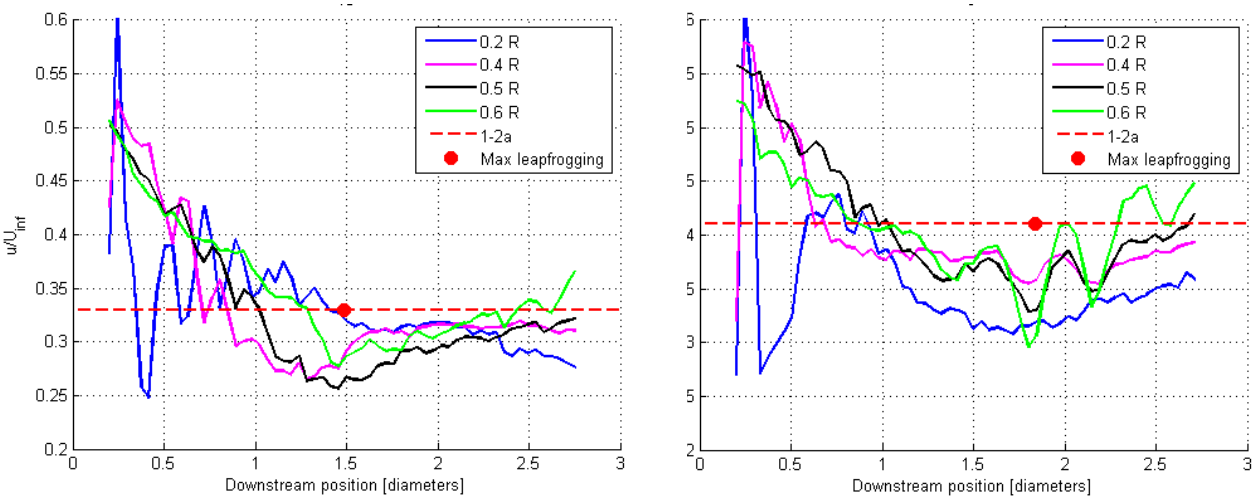

Figure 6: streamwise profiles of normalized phase locked axial velocity field $\langle u \rangle / U_{inf}$ at 4 different radial locations compared with the momentum theory value at the maximum wake expansion $U_{wake} = U_{inf}(1-a)$ at two different tip-speed ratios; (left)TSR=6; (right)TSR=4.8. The red dot indicates the location of the "maximum leapfrogging" in that phase, when the vortex filaments are one on top of each other.

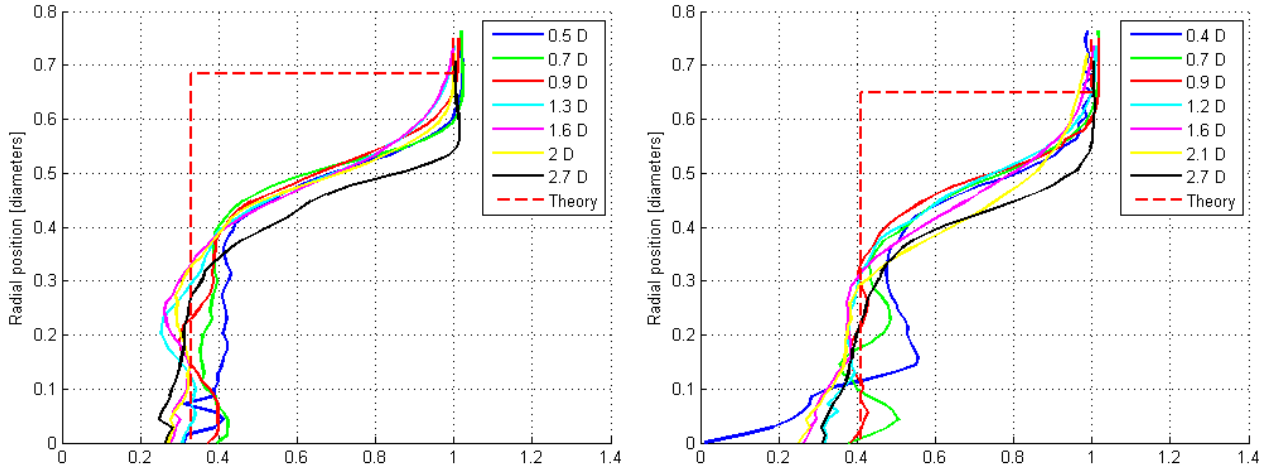

Figure 7: vertical profiles of normalized phase locked axial velocity field $\langle u \rangle / U_{inf}$ at 7 different downstream locations compared with the momentum theory profile at two different tip-speed ratios; (left)TSR=6; (right)TSR=4.8.

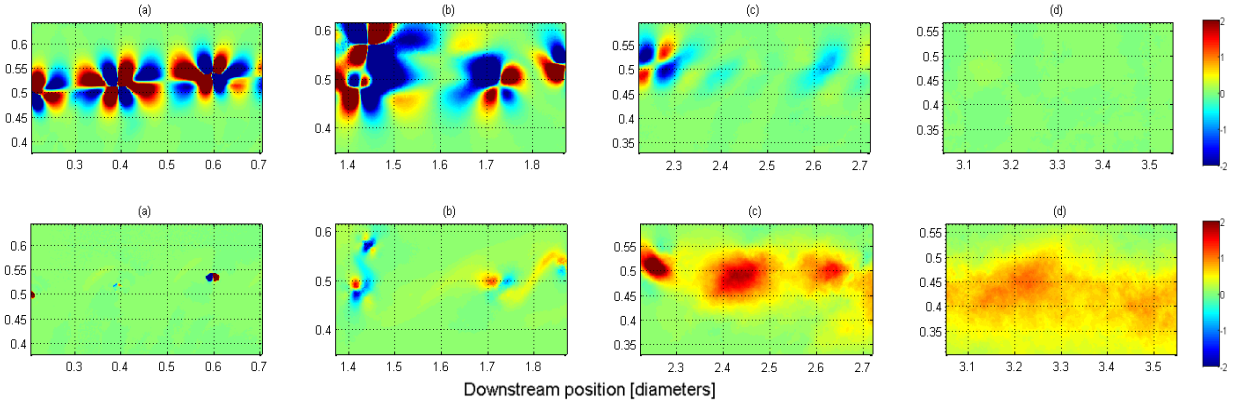

Figure 8:flux of mean flow kinetic energy [m^3/s^3] $\bar{u}\langle u'v'\rangle$ in one phase at 4 different downstream locations at TSR=6; (up) flux due to periodic (coherent) fluctuations; (down) flux due to random (incoherent) fluctuations

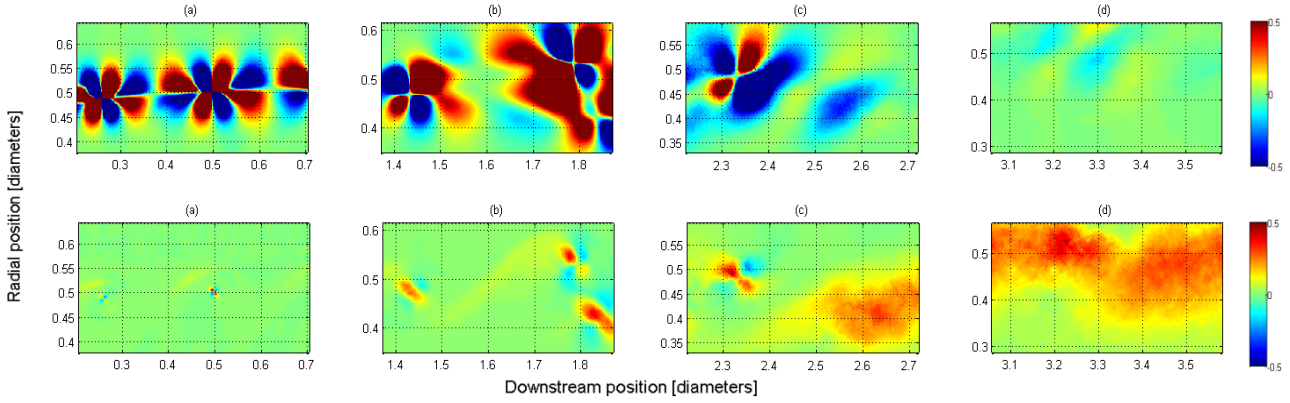

Figure 9: flux of mean flow kinetic energy [m^3/s^3] $\bar{u}\langle u'v'\rangle$ in one phase at 4 different downstream locations at TSR=4.8; (up) flux due to periodic (coherent) fluctuations; (down) flux due to random (incoherent) fluctuations

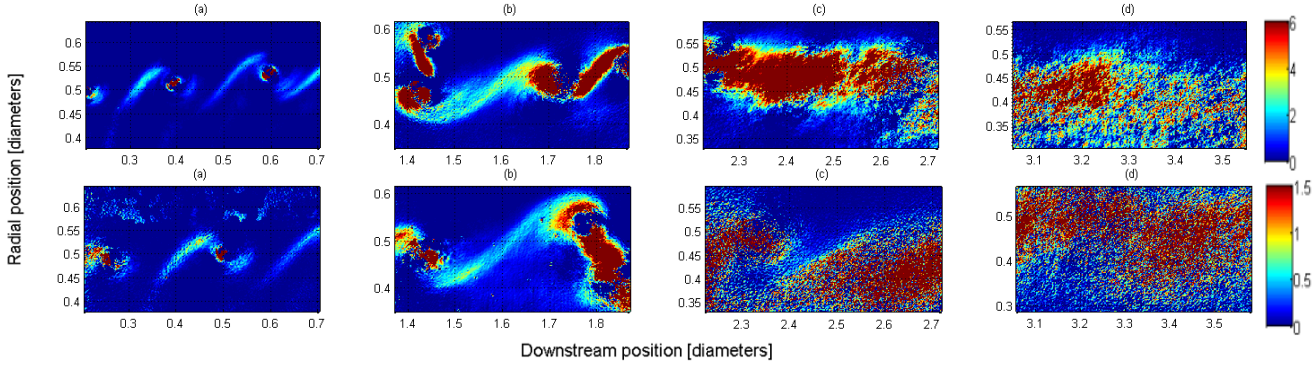

Figure 10: production of turbulent kinetic energy $\langle Pe\rangle = -u'^2\frac{\partial\langle u\rangle}{\partial x} - v'^2\frac{\partial\langle v\rangle}{\partial y} - u'v'\left(\frac{\partial\langle u\rangle}{\partial y} + \frac{\partial\langle v\rangle}{\partial x}\right)$ in one phase at 4 different downstream locations at two different tip-speed ratios; (up)TSR=6; (down)TSR=4.8

Conclusions and future work

The wake of a 60-centimetres HAWT has been measured with SPIV and analysed in order to investigate a relationship between the wake recovery and the evolution and instability of the tip-vortex helix. Unconditioned and phase-locked sampling of the velocity field have been conducted up to 2.7 diameters downstream in order to show the average field as well as the evolution of the tip vortices and their pairwise interaction. The main observation is a clear dependency of the onset of the instability on the value of TSR according to [3] and a strong influence of the leapfrogging event on the re-energising process of the wake. The finding is in accordance with the hypothesis of [7] who stated that the near wake tip-vortices are acting as a shield preventing the wake to mix with the outer flow. As last it is shown how the transport of the mean flow kinetic energy in the wake shear layer changes after the wake breakdown. The study suggests the possibility of a rotor design process which does not only take into account the aerodynamic and power optimisation of the rotor, but also the re-energising properties of the wake, in order to obtain more unstable and faster re-energising wakes. In the near future, the same experiment will be performed with a porous disc for simulating the actuator disc case and to show the differences in the process of kinetic energy entrainment and destruction along the two wake's in order to cast more light on the limitations in the current wake models based on the actuator disc assumption.

REFERENCES

[1] Barthelmie, R.J., Rathmann, O., Frandsen, S.T., Hansen, K.S., Politis, E., Prospathopoulos, J., Rados, K., Cabezón, D., Schlez, W., Phillips, J., Neubert, A., Schepers, J.G., van der Pijl, S.P., 2007. Modelling and measurements of wakes in large wind farms. Journal of Physics: Conference Series 75, 012049.

[2] Cal, R.B., Lebrón, J., Castillo, L., Kang , H.S., Meneveau, C., 2010. Experimental study of the horizontally averaged flow structure in a model wind-turbine array boundary layer. Journal of Renewable and Sustainable Energy 2.

[3] Felli, M., Camussi, R., Di Felice, F., 2011. Mechanisms of evolution of the propeller wake in the transition and far fields. Journal of Fluid Mechanics 682, 5-53.

[4] Hamilton, N., Kang, H.S., Meneveau, C., Cal, R.B., 2012. Statistical analysis of kinetic energy entrainment in a model wind turbine array boundary layer. Journal of Renewable and Sustainable Energy 4, 063105-063119.

[5] Hütter, U., 1977. Optimum Wind-Energy Conversion Systems. Annual Review of Fluid Mechanics 9, 399-419.

[6] Ivanell, S., Mikkelsen, R., Sørensen, J.N., Henningson, D., 2010. Stability analysis of the tip vortices of a wind turbine. WIND ENERGY 13, 705-715.

[7] Medici, D., 2005. Experimental Studies of Wind Turbine Wakes – Power Optimisation and Meandering, Mechanics. Royal Institute of Technology (KTH), Stockholm.

[8] Reynolds, W.C., Hussain, A.K.M.F., 1972. The mechanics of an organized wave in turbulent shear flow. Part 3. Theoretical models and comparisons with experiments. Journal of Fluid Mechanics 54, 263-288.

[9] Schepers, J.G., 2012. Engineering models in wind energy aerodynamics, Aerospace Engineering. Delft University of Technology.

[10] Selig, M.S., Guglielmo, J.J., Broeren, A.P., Giguère, P., 1995. Summary of Low-Speed Airfoil Data, in: Beach, V. (Ed.), Virginia Beach, VA, p. 292.
[11] Sorensen, J.N., 2011. Instability of helical tip vortices in rotor wakes. Journal of Fluid Mechanics.
[12] Westerweel, J., 1997 Fundamentals of digital particle image velocimetry. Measurement Science and Technology 8, 1379–1392.